ISSN 1070-3632, Russian Journal of General Chemistry, 2022, Vol. 92, No. 5, pp. 914–924. © Pleiades Publishing, Ltd., 2022.

Cyclization Reaction of 3,5-Diacetyl-2,6-dimethylpyridine with Salicylic Aldehyde and Its Derivatives: Quantum-Chemical Study and Molecular Docking

A. L. Stalinskaya[a], S. Y. Chikunov[a], I. A. Pustolaikina[b], and I. V. Kulakov[a,*]

[a] *Institute of Chemistry, Tyumen State University, Tyumen, 625003 Russia*
[b] *Buketov Karaganda University, Karaganda, 100024 Kazakhstan*
**e-mail: i.v.kulakov@utmn.ru*

Received April 17, 2022; revised April 29, 2022; accepted May 5, 2022

Abstract—Computational study of some details of the cyclization reaction between 3,5-diacetyl-2,6-dimethylpyridine and salicylic aldehyde in an acidic medium was performed by the DFT RB3LYP/6-31G method using the Gaussian-2016 software package. It was shown that protonation of the pyridine nitrogen atom leads to a significant increase in the charge of the hydrogen atom of the 2-methyl group of pyridine and the methyl acetyl group. This leads to the growth of the methyl group CH-acidity and enolization of the acetyl group. It was also found that the protonated tautomeric enol form of 3,5-diacetyl-2,6-dimethylpyridine gives a stable pre-reaction complex with salicylic aldehyde due to the formation of three hydrogen bonds. The formation of this pre-reaction complex, apparently, leads to the implementation of the Knoevenagel reaction, instead of the alternative possible Claisen–Schmidt reaction of salicylic aldehyde at the acetyl group of pyridine. The possible biological activity of the previously obtained cyclization products was evaluated by molecular docking using the AutoDock Vina software. Some cyclization products showed higher values of the binding affinity with the selected target proteins in comparison with the known antiviral drugs Nevirapine and Favipiravir. The results obtained confirm the correctness of the proposed cyclization mechanism between 3,5-diacetyl-2,6-dimethylpyridine and salicylic aldehyde. This also makes it possible to assess the prospects of previously obtained derivatives of epoxybenzo[7,8]oxocino[4,3-*b*]-pyridine as synthetic analogs of natural integrastatins A, B for further synthesis and study of their antiviral activity.

Keywords: integrastatins A and B, 3,5-diacetyl-2,6-dimethylpyridine, intramolecular cyclization, tetracyclic epoxybenzooxocine, molecular modeling, reaction mechanism, molecular docking

DOI: 10.1134/S107036322205022X

INTRODUCTION

Earlier, upon modification of 3,5-diacetyl-2,6-dimethylpyridine **1** into symmetric α,β-unsaturated ketones (bisazachalcones) **2** [1, 2], we have obtained an unexpected result [3]. To our surprise, 1-{(5*S*,11*S*)-2,5-dimethyl-11,12-dihydro-5*H*-5,11-epoxybenzo[7,8]-oxocino[4,3-*b*]pyridin-3-yl}ethan-1-one **3a** was obtained as the product of intramolecular cyclization in the Claisen–Schmidt aldol-croton condensation reaction between 3,5-diacetyl-2,6-dimethylpyridine **1** and salicylic aldehyde under acid catalysis conditions (in the presence of catalytic amounts of hydrochloric or trifluoroacetic acid) (Scheme 1) [3]. This compound, which is a structural analogue of integrastatins with an epoxybenzooxocin fragment [4, 5], was obtained instead of the expected α,β-unsaturated ketones **2** (as it was shown by the example of basic catalysis with other aromatic aldehydes, such as furfural, benzaldehyde, thiophenecarbaldehyde, 4-dimethylaminobenzaldehyde, 3,4-dimethoxybenzaldehyde and even 2-hydroxy-5-bromobenzaldehyde).

Integrastatins are natural compounds, which have shown a wide range of biological properties, including antimicrobial, antifungal, antioxidant, antitumor, and antiviral activity [6]. Therefore, many scientists have been actively started the development of synthetic methods of the benzooxocine tetracyclic nucleus formation since about 2003 [7–14].

Previously, we have studied in detail and optimized the synthesis of 5*H*-5,11-epoxybenzo[7,8]oxocino[4,3-*b*]-

Scheme 1.

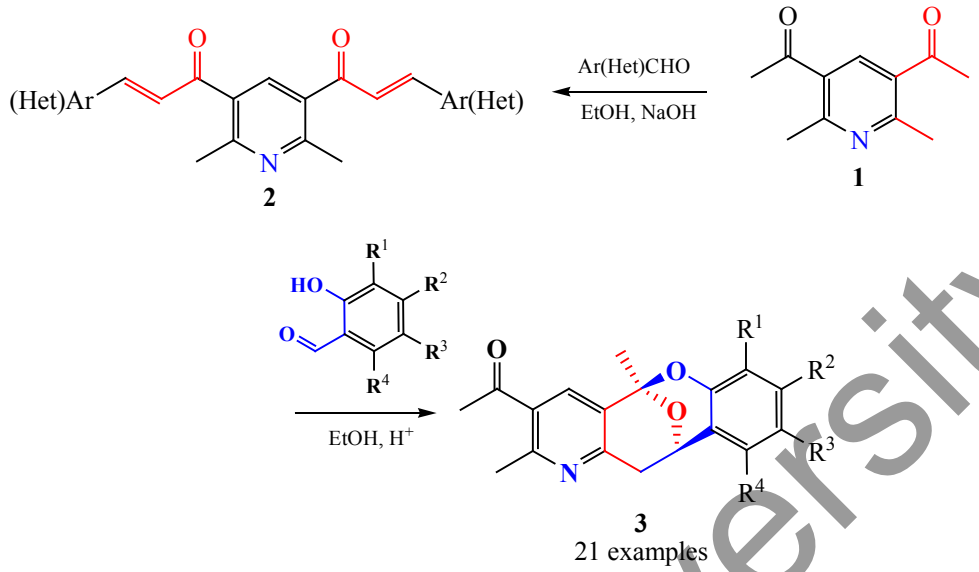

pyridine derivatives as new structural analogs of integrastatins. We considered this reaction by the example of the 1-{(5*S*,11*S*)-2,5-dimethyl-11,12-dihydro-5*H*-5,11-epoxybenzo[7,8]oxocino[4,3-*b*]pyridin-3-yl}ethan-1-one **3a** formation from 3,5-diacetyl-2,6-dimethylpyridine **1** and salicylic aldehyde [3]. The reaction tolerates a large number of substituted salicylic aldehydes (Scheme 1).

Currently, we are comprehensively and widely studying the cyclization possibilities of other substituted 3-acetyl-2-methylpyridines and their diaza analogs with the salicylic aldehyde.

In general, we have accumulated a fairly large amount of experimental material on the previously undescribed cyclization of pyridine **1** with the salicylic aldehyde. It seemed promising to apply modern computational methods to understand which features influence the specific course of the studied cyclization reaction and to comprehend the importance of the results obtained. This will make it possible to consider step by step the cyclization process by quantum chemical methods, as well as to evaluate the possible biological activity of the previously obtained cyclization products using molecular docking.

COMPUTATIONAL METHODS

Methods and techniques for the molecular modeling of the cyclization reaction mechanism. We applied quantum-chemical methods to simulate some intermediates of the studied cyclization between pyridine **1** and salicylic aldehyde **2**. We took the DFT RB3LYP method in the 6-31G basis and semiempirical AM1 method using the Gaussian-2016 software package [15]. BLYP exchange-correlation functional is one of the most widespread in modern quantum chemical calculations. The B3LYP approximation is based on a hybrid functional in which the exchange energy is calculated using the exact result obtained by the Hartree–Fock method [16–18]. The spin states of the calculated structures were taken into account on the basis of the Restricted Hartree-Fock method (RHF), since the objects under study have closed electron shells. The correctness of the accepted calculation method was verified by comparing the calculated and experimental data of single crystal X-ray diffraction analysis (CCDC 2035579, Fig. 1), namely bond lengths for 1-{(5*S*,11*S*)-2,5-dimethyl-11,12-dihydro-5*H*-5,11-epoxybenzo[7,8]oxocino[4,3-*b*]pyridin-3-yl}ethan-1-one as the target cyclization product (Table 1).

As can be seen from the data presented in Table 1, the difference in bond lengths is within 0.04 Å or does not exceed 3.5%, which indicates the adequacy of the chosen method of quantum-chemical calculation.

The molecular structure of the calculated objects we built manually in the GaussView 6.0 graphical editor [19]. After that, we optimized the geometry using the selected method without any restrictions. Then, we evaluated

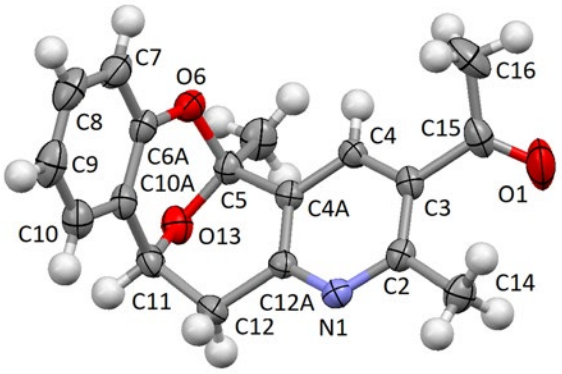

Fig. 1. ORTEP representation of the molecular structure of compound **3a**.

the geometric, energy and charge characteristics of the calculated objects based on the data obtained.

The progress of the cyclization reaction we modeled in two stages. We applied the QST2 procedure to find the transition state, the IRC procedure to obtain the reaction energy profile, and estimate the activation energy for the stage 1 simulations using the DFT RB3LYP/6-31G method. The pre-reaction complex formation modeling for stage 2 we carried out by the AM1semiempirical method. We have applied a semiempirical method here because it takes into account hydrogen bonds well6 whereas the use of the DFT RB3LYP/6-31G method did not allow us to fix the complex of the required configuration.

All calculations were performed without taking into account the effect of the solvent (gas phase, vacuum).

Molecular docking. We applied molecular docking to study the predicted biological activity of some products of the cyclization reaction (Scheme 1). Molecular docking studies simulate the interactions between ligand and receptors. These interactions between the ligand and the receptor make it possible to predict biological activity of new substances [20].

We took HIV-1 reverse transcriptase (3V81) [21] and SARS-CoV2 RNA-dependent RNA polymerase (7AAP) [22] as target proteins. All the structures were taken from the Protein Databank (PDB) [23]. Protein structures were prepared for docking by removing water molecules, the native ligand, and adding polar hydrogen atoms. Then they were converted to pdbqt format using the AutoDock MGL software package [24]. Docking was performed using AutoDock Vina software [25]. Visualization and analysis of the results obtained were carried out using the Discovery Studio software package [26]. The grid coordinates of the active site were used for the structure of HIV-1 reverse transcriptase (3V81) (x = 1.561, y = –32.788, z = 22.677). The following grid coordinates of the receptor active site were used for the structure of SARS-CoV2 RNA-dependent RNA polymerase (7AAP): (x = 100.953, y = 95.578, z = 111.984). The following native ligands were used to compare the free energies (kcal/mol) of the resulting complexes: Nevirapine as a synthetic antiviral drug from the group of non-nucleoside

Table 1. Some bond lengths in the molecule of compound **3a** according to single crystal X-ray diffraction and DFT calculation data (RB3LYP 6-31G)

Bond	Bond length, Å		Absolute error, Å	Relative error, %
	PCA	RB3LYP 6-31G		
N^1–C^2	1.3411	1.35383	0.01273	0.94
C^3–$C1^5$	1.5042	1.49001	0.01419	0.94
C^5–O^6	1.4472	1.48048	0.03328	2.29
O^6–C^{6A}	1.3798	1.40020	0.02040	1.47
N^1–C^{12A}	1.3447	1.35014	0.00544	0.40
O^1–C^{15}	1.2101	1.24919	0.03909	3.23
C^5–O^{13}	1.4075	1.43966	0.03216	2.28
C^{11}–O^{13}	1.4406	1.47891	0.03831	2.65
C^2–C^3	1.4058	1.42515	0.01935	1.37
C^{15}–C^{16}	1.493	1.51951	0.02651	1.77
C^{4A}–C^5	1.5272	1.52507	0.00213	0.13
C^{4A}–C^{12A}	1.3939	1.40509	0.01119	0.80

Scheme 2.

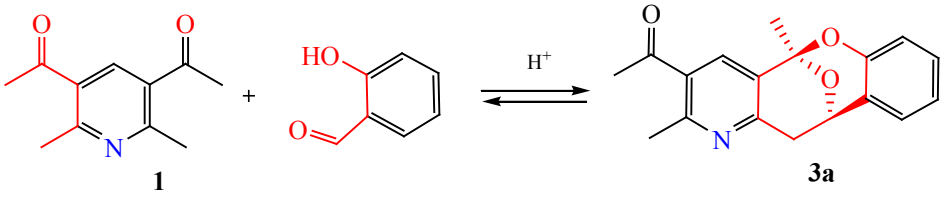

Scheme 3.

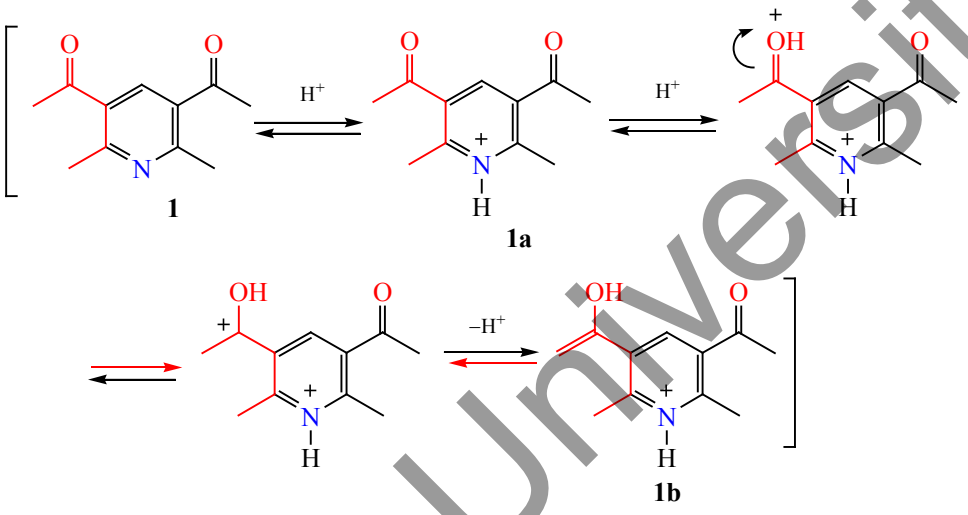

reverse transcriptase inhibitors (it is used for the treatment and prevention of HIV / AIDS, in particular HIV-1) for 3V81 [21]; and Favipiravir as antiviral agent (it is being investigated as a possible remedy against SARS-CoV-2) for 7AAP [22]. These native ligands have also been docked to corresponding proteins.

RESULTS AND DISCUSSION

Molecular modeling of the cyclization reaction mechanism. Based on the obtained experimental data, as well as the analysis of literature, we have previously proposed the following possible mechanism of cyclization between pyridine **1** and salicylic aldehyde (Scheme 2) [3].

This mechanism can be conditionally divided into two stages: (1) isomerization of 3,5-diacetyl-2,6-dimethylpyridine **1** in an acidic medium (Scheme 3) and (2) cyclization of the protonated tautomeric enol form of 3,5-diacetyl-2,6-dimethylpyridine **1b** with salicylic aldehyde (Scheme 4).

Initially, we designed and optimized the geometry of the initial substances (3,5-diacetyl-2,6-dimethylpyridine **1**, salicylic aldehyde) and the cyclization reaction product (oxocin **3a**) (Table 2). As a result of geometry optimization, we obtained the structures of the most stable conformations, estimated the geometric, energy and Mulliken charge characteristics for all three molecules (Table 2). It can be seen from the charges distribution in the molecule **1** that the methyl groups both in the 2-, 6-pyridine position and in the acetyl group have sufficient CH acidity. It can also be noted that the acetyl group (**1**) is characterized by higher values of the positive charge on hydrogen atoms, which indicates its higher acidity and shows the possibility of a side Claisen–Schmidt reaction through it. In addition, the concentration of a relatively large positive charge (+0.179) on the hydrogen atom of the acetyl group promotes the formation of an intramolecular hydrogen bond with an adjacent oxygen atom having a charge of –0.403. This in turn promotes the formation of the tautomeric enol form of the molecule **1b** in accordance with the stage 1.

Scheme 4.

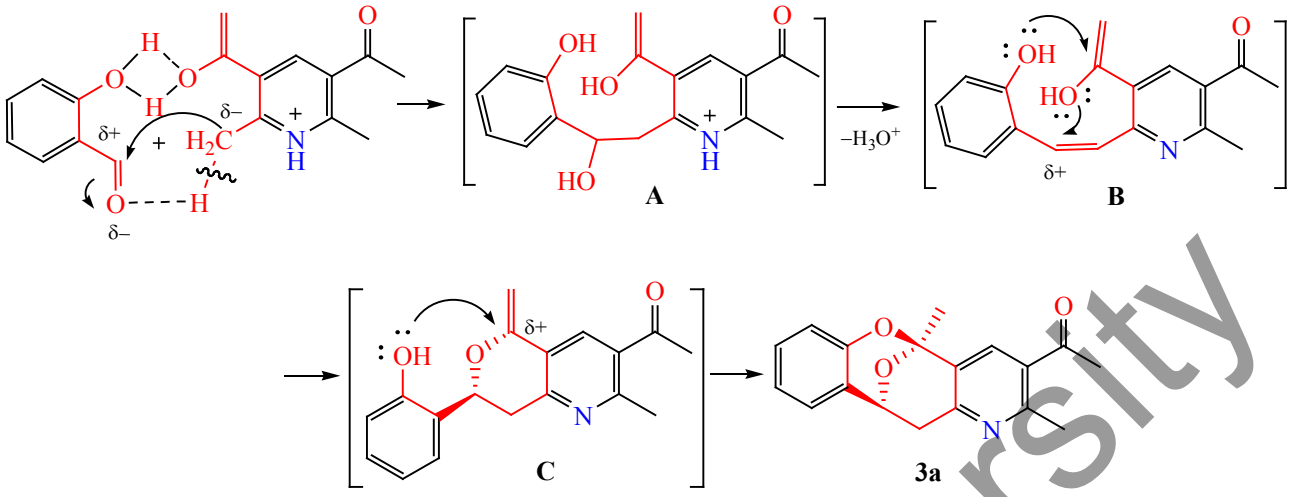

Table 2. Optimized geometry and calculated charge characteristics of salicylic aldehyde, compounds **1** and **3a**

Compound	Structural formula	Optimized geometry and Mulliken charges
3,5-Diacetyl-2,6-dimethylpyridine **1**	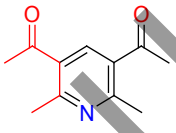	
Salicylic aldehyde	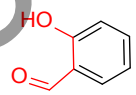	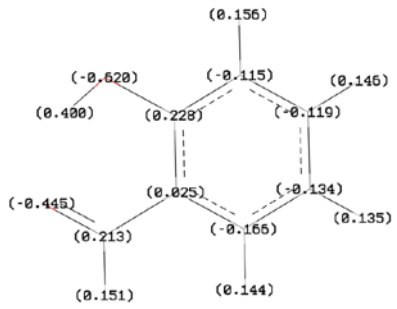
Oxocin **3a**	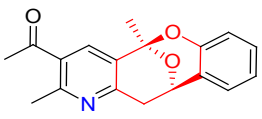	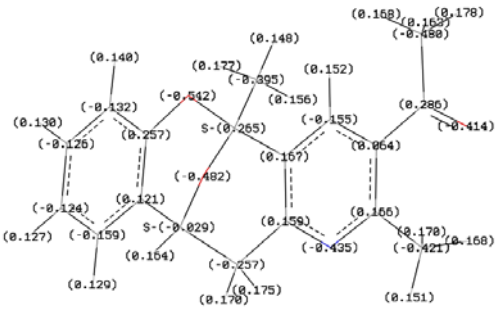

Table 3. Optimized geometry and some calculated characteristics of structures of the stage 1

Compound	Structural formula	Optimized geometry and Mulliken charges	E_{total}, a.u.
3,5-Diacetyl-2,6-dimethylpyridine (**1**)	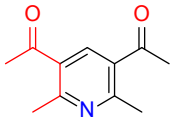		–632.0234
Protonated form of 3,5-diacetyl-2,6-dimethylpyridine (**1a**)	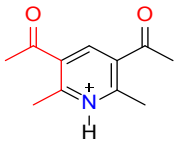	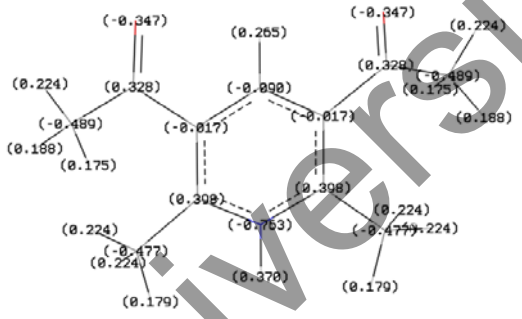	–632.4010
Double protonated form of 3,5-diacetyl-2,6-dimethylpyridine (**1a**$^{+}$)	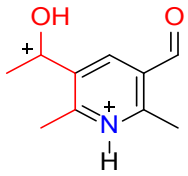	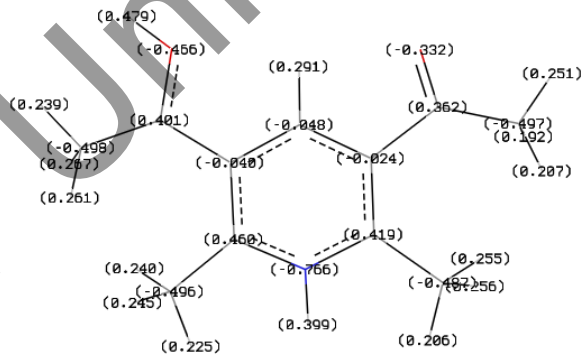	–632.6083
Enol form of 3,5-diacetyl-2,6-dimethylpyridine (**1b**)	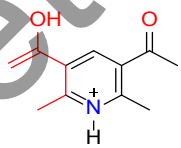	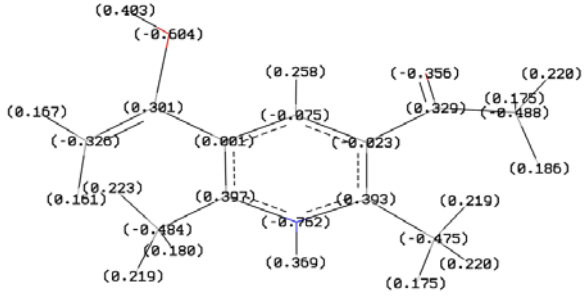	–632.3911

The next step we performed modeling of the geometry of the protonated form **1a** since stage 1 proceeds in an acidic medium (Table 3). Protonation was carried out at the nitrogen atom, taking into account the +1 charge for the calculated structure. As can be seen from the data presented in Table 3, the positive charge on the hydrogen atom of the 2-methyl and acetyl groups of the protonated form of pyridine **1a** increased to +0.224. This indicates

Scheme 5.

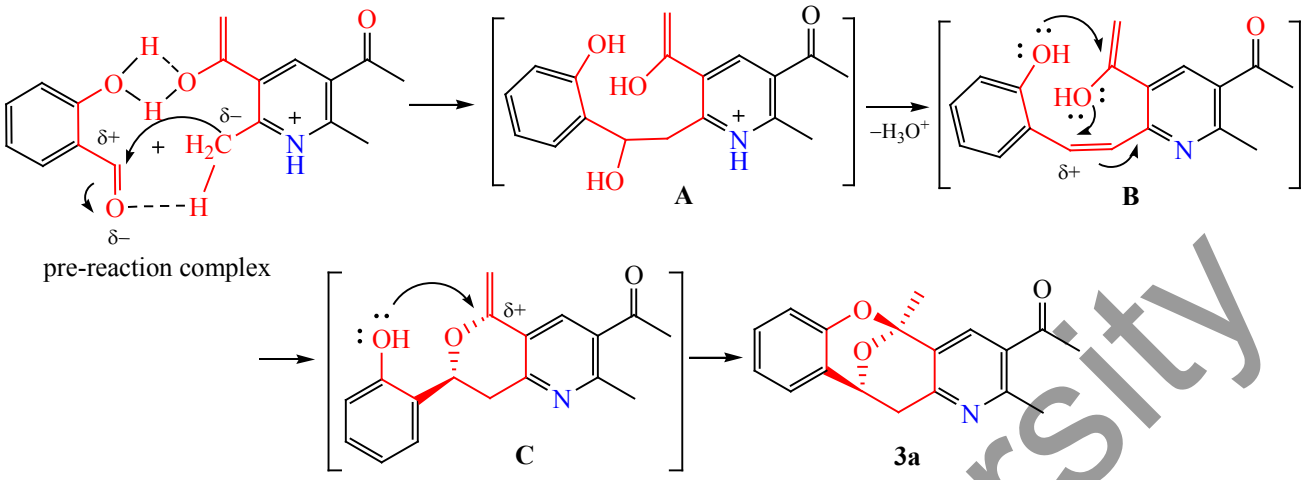

Scheme 6.

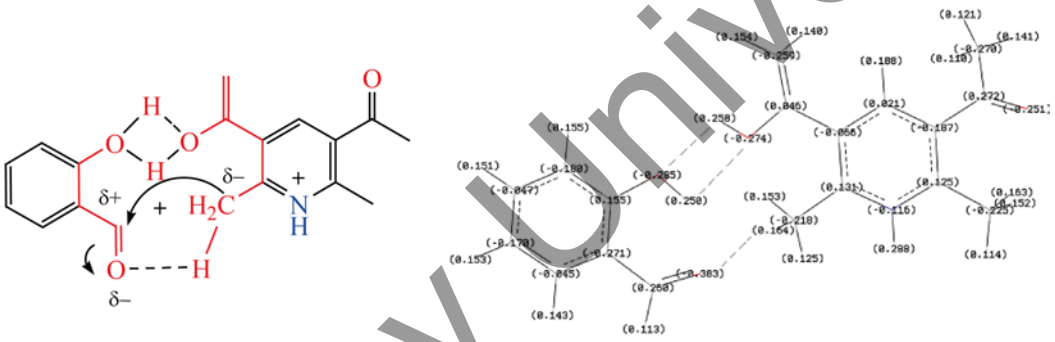

a higher CH acidity of **1a** compared to the pyridine molecule **1**.

The total proton energy is zero in quantum chemical calculations, so we can compare the total energies of the molecule **1** (E_{total} = –632.0234 a.u.) and its protonated form **1a** (E_{total} = –632.4010 a.u.). It was shown that the protonated form is thermodynamically more stable (ΔE_{1a} = 0.3776 a.u. = 236.9451 kcal/mol[1]*). The total energies of structures $\mathbf{1a}^+$ and **1a** correlate in a similar way (ΔE_{1a^+} = 0.2072 a.u. = 130.0476 kcal/mol). This can be interpreted as the thermodynamic profitability of the process. The splitting off of a proton during the transition from $\mathbf{1a}^+$ to **1b** requires the energy consumption ΔE_{1b} = 0.2172 a.u. = 136.3162 kcal/mol. This value is covered by an excess of energy released during the first two transitions (ΔE_{1a} +ΔE_{1a^+}). In general, it can be concluded that stage 1 is a spontaneous process under study conditions.

Thus, based on quantum-chemical modeling of the stage 1, the possibility of its proceeding according to the proposed mechanism with preliminary protonation of pyridine **1** at the nitrogen atom and subsequent protonation of the carbonyl group has been shown. This process should be spontaneous due to the energy released during protonation.

To further study the progress of the cyclization reaction between pyridine **1** and salicylic aldehyde, we performed quantum-chemical modeling of the pre-reaction complex for stage 2 (Scheme 5).

The configuration of this complex is favorable for the cyclization reaction. We succeeded in fixing this complex using the AM1 semiempirical method, which most fully takes into account the effect of hydrogen bonds. Optimized geometry and charge characteristics of

[1] 1 a.u. = 627.503 kcal/mol.

Scheme 7.

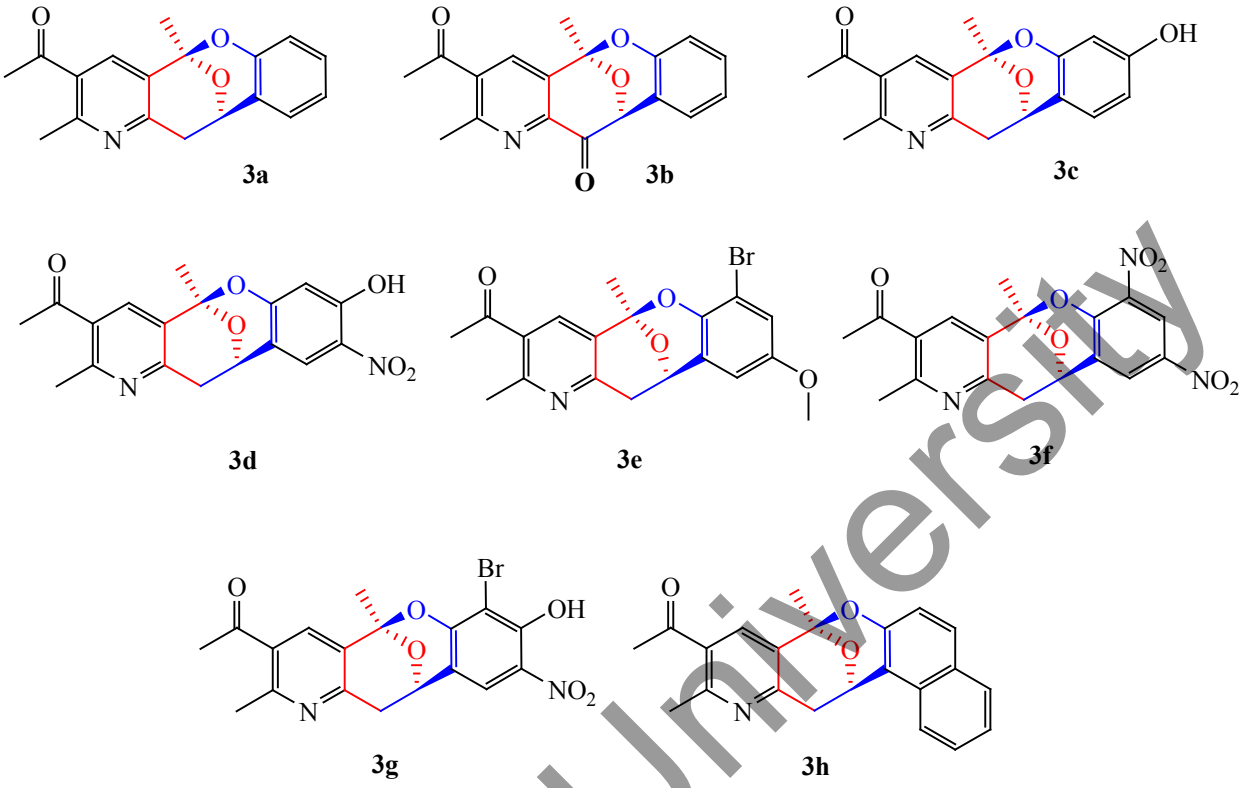

pre-reaction complex formed at the stage 2 is represented in Scheme 6.

As can be seen from the structure shown in Scheme 6, the pre-reaction complex is characterized by the formation of hydrogen bonds between the reaction sites: two practically equivalent hydrogen bonds are formed between the OH groups of the interacting molecules **1b** and salicylic aldehyde. Adduct **A** is formed as a result of further nucleophilic attack of the methyl group carbon at the carbonyl carbon of salicylic aldehyde by the Knoevenagel reaction. Ylidene **B** is formed by dehydration of water from adduct **A**. Then, first, one –C–O–C– bond is formed as a result of the Michael reaction of the OH-group of the enol form of the acetyl group of **1b** with the more electrophilic carbon atom of the double bond of ylidene **B**. After that there is a second cross-nucleophilic Michael addition between the OH group of the aldehyde residue and the more electrophilic vinyl carbon atom of the tetrahydro-2*H*-pyran ring. At the end, ring- closing occurs to form benzooxocin core.

Molecular docking of cyclization reaction products. The new heterocyclic (tetracyclic benzooxocino[4,3-*b*]-pyridine) system may be of great potential interest in terms of possible antiviral activity. To check this assumption, we carried out molecular docking of several representatives of the previously synthesized oxocino[4,3-*b*]pyridine derivatives **3a–3h** (Scheme 7) [3].

Evaluation of the binding affinity (kcal/mol) with the selected receptors showed that this value is higher for the studied structures in comparison with native ligands (Table 4). It was also found that the presence of carbonyl oxygen at the 12-position in compound **3b** increases its affinity for the selected receptors compared to compound **3a**.

An analysis of the interactions of the 3V81 protein and ligand **3h** in the complex was performed. It showed that the ligand molecule is oriented through two Pi-Sigma interactions with the DT812 and DC713 nucleotide fragments, two Pi–Pi T bonds with the DC712 nucleotide fragment, and there are two Pi-alkyl interactions with ARG356 and one hydrogen bond with ARG356. In

Table 4. Binding affinity (kcal/mol) for complexes of proteins 3V81 and 7AAP with native ligands and compounds **3a**–**3h**

Ligand	3V81	7AAP
Nevirapine	–7.5	–
Favipiravir-RTP	–	–6.3
3a	–7.9	–6.2
3b	–8.1	–7.4
3c	–8.2	–7.6
3d	–8.6	–7.5
3e	–8.6	–7.4
3f	–8.7	–8.0
3g	–8.8	–8.2
3h	–9.1	–8.0

addition, ten van der Waals interactions with amino acid residues GLU514, ALA360, MET357, GLY359, ARG358 and nucleotide fragments DG714, DA715, DG811, DT813 and DC814 were found (Fig. 2).

The study of the interactions of the 7AAP protein and **3g** ligand in the complex was carried out. It was shown that the ligand forms one C ***H bond with SER682, one Pi-Sigma interaction with nucleotide fragments A11, four van der Waals interactions with amino acid residues THR687, ASP 760 and nucleotide fragments C10, U20, as well as two metal-acceptor interactions with MG101 and MG1003 magnesium atoms (Fig. 3).

CONCLUSIONS

In summary, the correctness of the previously suggested cyclization mechanism between 3,5-diacetyl-2,6-dimethylpyridine and salicylic aldehyde in an acidic medium was confirmed by quantum-chemical calculations. For example, protonation of the pyridine nitrogen atom leads to a significant increase in the charge on the hydrogen atom (from +0.160 to +0.224) of the 2-methyl group of pyridine and the methyl acetyl group. This, in turn, initiates an increase its CH-acidity, as well as the required enolization of the acetyl group. The formation of a favorable configuration of the pre-reaction complex of the protonated tautomeric enol form of 3,5-diacetyl-2,6-dimethylpyridine and salicylic aldehyde is facilitated by three hydrogen bonds. Apparently, the formation of this pre-reaction complex leads to the Knoevenagel reaction instead of the alternative Claisen–Schmidt reaction of salicylic aldehyde at the acetyl group of pyridine (it is side reaction in this case). For example, we have earlier obtained azachalcones by-product in a neutral medium as a result of the Claisen–Schmidt reaction [3].

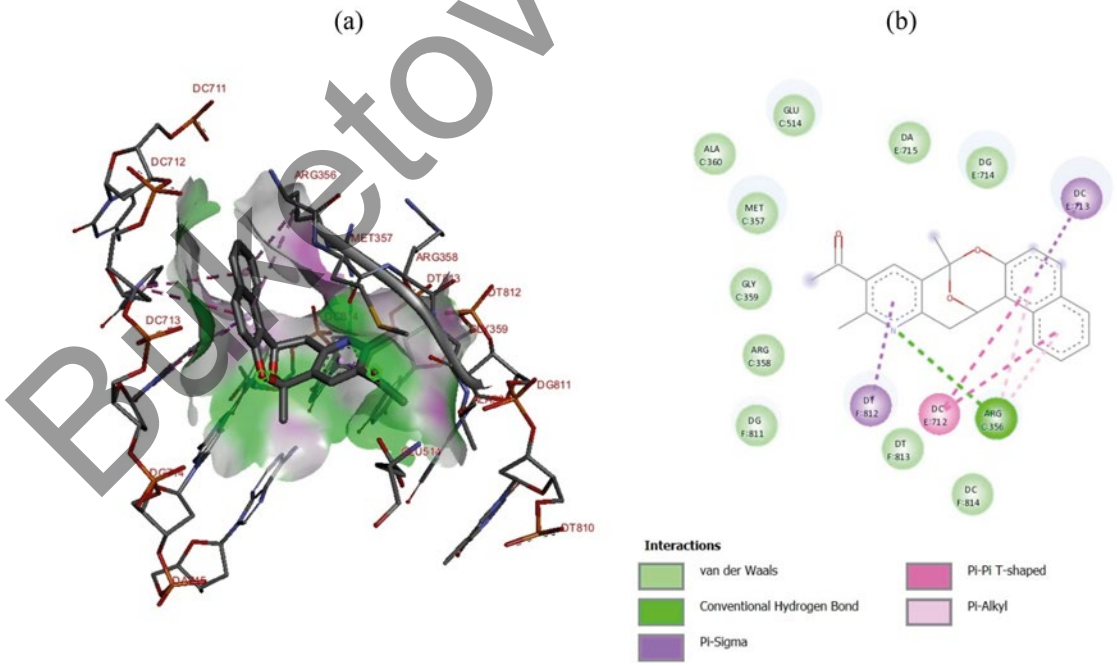

Fig. 2. Complex between oxocino[4,3-*b*]pyridine **3h** and HIV-1 reverse transcriptase (3V81). (a) 3D Docking model and (b) 2D docking model.

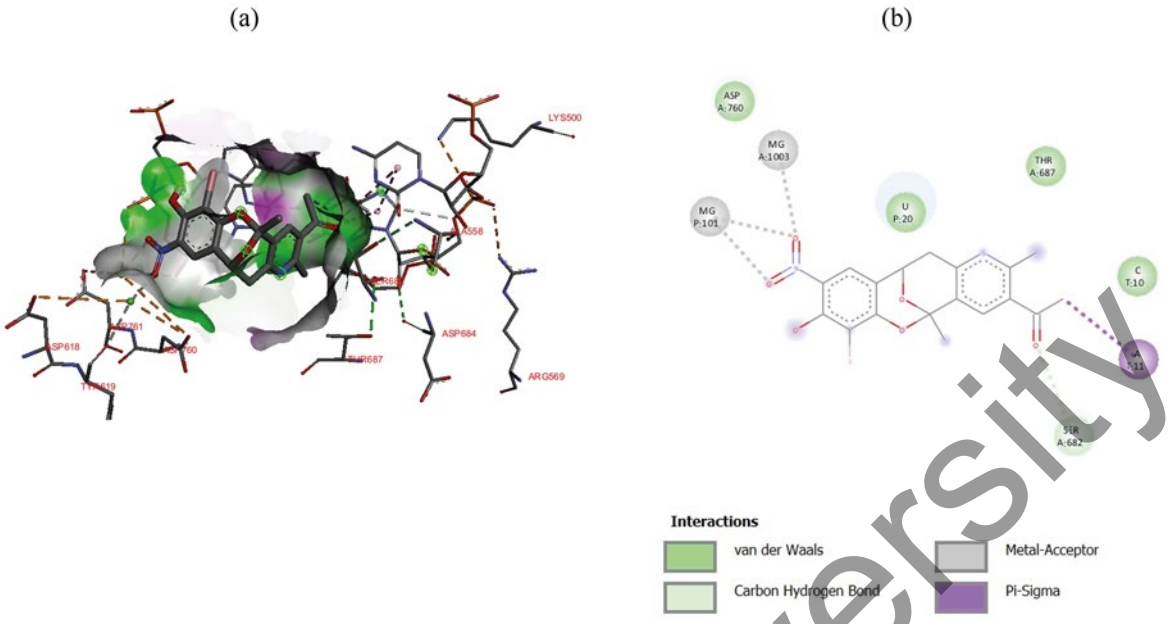

Fig. 3. Complex between oxocino[4,3-*b*]pyridine **3g** and SARS-CoV2 RNA dependent RNA polymerase (7AAP). (a) 3D Docking model and (b) 2D docking model.

The results of molecular docking of the formed oxocino[4,3-*b*]pyridine derivatives showed their higher binding energy with the selected target proteins in comparison with the antiviral drugs Nevirapine and Favipiravir. This showed that these compounds are promising for further study of their possible antiviral activity. An increase in the free energies of complexes with target proteins was also noted for structure, which has a carbonyl group at the 12th position of the oxocin nucleus (as in the molecules of natural integrastatins A, B), as compared to its unoxidized form.

CONFLICTS OF INTEREST

No conflict of interest was declared by the authors.

FUNDING

This work was financially supported by the Russian Science Foundation (grant no. 22-23-01015).

REFERENCES

1. Kulakov, I.V., Karbainova, A.A., Shulgau, Z.T., Seilkhanov, T.M., Gatilov, Y.V., and Fisyuk, A.S., *Chem. Heterocycl. Compd.*, 2017, vol. 53, p. 1094. https://doi.org/10.1007/s10593-017-2178-6
2. Oleshchuk, A.L., Karbainova, A.A., Krivoruchko, T.N., Shulgau, Z.T., Seilkhanov, T.M., and Kulakov, I.V., *Chem. Heterocycl. Compd.*, 2019, vol. 55, p. 47. https://doi.org/10.1007/s10593-019-02417-5
3. Kulakov, I.V., Stalinskaya, A.L., Chikunov, S.Y., and Gatilov, Y.V., *New J. Chem.*, 2021, vol. 45, p. 3559. https://doi.org/10.1039/D0NJ06117D
4. Talontsi, F.M., Dittrich, B., Schuffler, A., Sun, H., and Laatsch, H., *Eur. J. Org. Chem.*, 2013, vol. 2013, p. 3174. https://doi.org/10.1002/ejoc.201300146
5. Amrani, M.El, Lai, D.W., Debbab, A., Aly, A.H., Siems, K., Seidel, C., Schnekenburger, M., Gaigneaux, A., Diederich, M., Feger, D., Lin, W.H., and Proksch, P., *J. Nat. Prod.*, 2014, vol. 77, p. 49. https://doi.org/10.1021/np4005745
6. Oumzil, H., Ghoulami, S., Rhajaoui, M., Ilidrissi, A., Fkih-Tetouani, S., Faid, M., and Benjouad, A., *Phytother. Res.*, 2002, vol. 16, p. 727. https://doi.org/10.1002/ptr.1045
7. Foot, J.S., Giblin, G.M.P., and Taylor, R.J.K., *Org. Lett.*, 2003, vol. 5, p. 4441. https://doi.org/10.1021/ol035786v
8. Foot, J.S., Giblin, G.M.P., Whitwood, A.C., and

Taylor, R.J.K., *Org. Biomol. Chem.*, 2005, vol. 3, p. 756. https://doi.org/10.1039/B418426B

9. Ramana, V., Reddy, C.N., and Gonnade, R.G., *Chem. Commun.,* 2008, vol. 27, p. 3151. https://doi.org/10.1039/B801755G
10. More, A. and Ramana, C.V., *Org. Lett.*, 2016, vol. 18, p. 612. https://doi.org/10.1021/acs.orglett.5b03707
11. More, A. and Ramana, C.V., *Org. Lett.*, 2016, vol. 18, p. 1458. https://doi.org/10.1021/acs.orglett.6b00404
12. Tadross, P.M., Bugga, P., and Stoltz, B.M., *Org. Biomol. Chem.*, 2011, vol. 9, p. 5354. https://doi.org/10.1039/C1OB05725A
13. Jeong, J.Y., Sperry, J., and Brimble, M.A., *J. Org. Chem.*, 2019, vol. 84, p. 11935. doi
14. Yamagiwa, Y. Haruna, N. Kawakami, H., and Matsumoto, K., *Bull. Chem. Soc. Jpn.*, 2020, vol. 93, p. 1036. https://doi.org/10.1246/bcsj.20200070
15. Frisch, M.J., Trucks, G.W., Schlegel, H.B., Scuseria, G.E., Robb, M.A., Cheeseman, J.R., and Fox, D.J., Gaussian 16, Revision B.01. Wallingford: Gaussian Inc., 2016. http://gaussian.com
16. Lee, T., Yang, W.T., and Parr, R.G., *Phys. Rev. B: Condens. Matter.*, 1988, vol. 37, p. 785. https://doi.org/10.1103/PhysRevB.37.785
17. Becke, A.D., *J. Chem. Phys.*, 1993, vol. 98, p. 1372. https://doi.org/10.1063/1.464304
18. Stephens, P.J., Devlin, F.J., Chabalowski, C.F., and Frisch, M.J., *J. Phys. Chem.*, 1994, vol. 98, p. 11623. https://doi.org/10.1021/j100096a001
19. Dennington, R., Keith, T., and Millam, J., GaussView, Version 6, Semichem Inc., Shawnee Mission, KS, 2016. http://gaussian.com.
20. Morris, G.M., Goodsell, D.S., Huey, R., and Olson, A.J., *J. Comp.-Aided Mol. Design*, 1996, vol. 10, p. 293. https://doi.org/10.1007/BF00124499
21. Das, K., Sarafianos, S.G., and Arnold, E., *Nature Struct. Mol. Biol.*, 2013, vol. 20, p. 1341. https://doi.org/10.1038/nsmb.2725
22. Naydenova, K., Muir, K.W., Wu, L.F., Zhang, Z.G., Coscia, F., Peet, M.J., Castro-Hartmann, P., Qian, P., Sader, K., Dent, K., Kimanius, D., Sutherland, J.D., Lowe, J., Barford, D., and Russo, C.J., *Proc. National Academy of Sciences of the United States of America*, 2021, vol. 118, p. e2021946118. https://doi.org/10.1073/pnas.2021946118
23. https://www.rcsb.org.
24. Morris, G.M., Huey, R., Lindstrom, W., Sanner, M.F., Belew, R.K., Goodsell, D.S., and Olson, A.J., *J. Comput. Chem.*, 2009, vol. 30, p. 2785. https://doi.org/10.1002/jcc.21256
25. Trott, O. and Olson, A.J., *J. Comput. Chem.,* 2010, vol. 31, p. 455. https://doi.org/10.1002/jcc.21334
26. Discovery Studio 2015: Dassault Systemes BIOVIA, Discovery Studio Modelling Environment, Release 4.5, San Diego: Dassault Systems.